PML controls angiogenesis and EMT to limit metastasis in MDAMB231 cells

Amalia P Vogiatzoglou[1,2], Sirago Spanou[1,2], Nikoleta Sachini[1,2,5], Elias Drakos[3], Christoforos Nikolaou[4], Takis Makatounakis[1], Androniki Kretsovali[1], Joseph Papamatheakis[1,2]

1 Institute of Molecular Biology and Biotechnology, FORTH, 70013 Heraklion, Crete, Greece.
2 Department of Biology, University of Crete, Vassilika Vouton, 70013 Heraklion, Greece
3 Department of Pathology, Medical School, University of Crete, Heraklion, Voutes, 71110 Crete, Greece
4 Biomedical Sciences Research Center "Alexander Fleming", Institute for Bioinnovation, 16672 Vari, Greece
5 ADC Therapeutics Limited, London, United Kingdom

Corresponding Author:
Joseph Papamatheakis
Email: papamath@imbb.forth.gr
Institute of Molecular Biology and Biotechnology (IMBB), Foundation for Research and Technology-Hellas (FORTH); Nikolaou Plastira 100 GR-70013, Heraklion, Crete GREECE.
Phone: +30-2810-391165,

Co-corresponing author:
Androniki Kretsovali
Email: kretsova@imbb.forth.gr
Institute of Molecular Biology and Biotechnology (IMBB), Foundation for Research and Technology-Hellas (FORTH); Nikolaou Plastira 100 GR-70013, Heraklion, Crete GREECE.
Phone: +30-2810-391191

SUMMARY

Breast cancer is a heterogeneous disease that underlies the divergent role of some regulatory factors on tumor biology. Here we studied PML, a factor with opposing context-dependent roles in cancer. We chose to Knock Down (KD) PML in MDAMB231 and MCF7 breast cancer cell lines that represent aggressive-mesenchymal (claudin–low) and non-aggressive, epithelial (luminal A) subtype respectively. We examined tumor cell physiology *in vitro* and by xenografting and sought to correlate the PML-KD effects with transcriptional changes. *In vitro* assays showed that PML loss exacerbated the aggressive properties of MDAMB231 cells only, in correlation with deregulation of cell-cycle and adhesion related genes. PML-KD xenografts had increased local growth and metastatic ability with a preference for the lung. We propose that in tumor xenografts, PML loss facilitates long-term maintenance of tumor initiating cells and unleashes a hypoxia-angiogenic switch. Thus, PML expression may serve as a useful breast cancer biomarker.

ABSTRACT

PML is the core protein of the cognate nuclear particles, called PML nuclear bodies (NBs), that regulate a large number of highly divergent and often opposing functions. Being originally shown to act as a tumor suppressor PML has been recently implicated in tumor survival and metastases. Using two different Breast Cancer cell types, MDAMB231 and MCF7 we observed highly cell type and growth context dependent regulation. In line with our transcriptional profiling, PML deficient MDAMB231 but not MCF7 cells show increased cell cycle and decreased cell adhesion related features consistent with a highly aggressive propensity. In agreement with this, PML KD tumor xenografts grew faster and had an increased metastatic activity with a preference for lung and to a lesser degree the liver. PML deficient primary and lung metastatic tumors expressed increased levels of the mesenchymal TWIST2 protein. Moreover both TWIST2 and SNAIL were shown to interact with different PML isotypes implying a possible role of PML in regulating their abundance and/or activity. Notably, PML loss in MDAMB231 cells led to an enhanced hypoxia-angiogenesis phenotype and metastasis of *in vivo* growing cells which aquare a gene expression profile resembling the earlier described lung metastasis signature. We propose that PML limits the *in vivo* emergence of aggressive and metastatic tumor phenotype. Mechanistically this is linked to the long term maintenance of tumor initiating cells, potentiation of their mesenchymal phenotype and a hypoxia-angiogenic switch.

KEYWORDS

PML, Breast cancer, tumor microenvironment, angiogenesis, hypoxia, HIF1a, EMT, TWIST2,

INTRODUCTION

Breast cancer is characterized by genetic and epigenetic complexity and phenotypic heterogeneity [1]. Differences between breast cancer-subtypes or patients referred as intertumoral heterogeneity as well as cellular diversity within the same tumors[2] is dynamically driven by genetic and epigenetic evolution and has an impact in patient's prognosis and therapy. Major current efforts are directed towards the elucidation of factors that modify the action of critical oncogene or tumor suppressor pathways that regulate invasiveness metastatic potential and drug response with predictive or therapeutic importance.

The Promyelocytic Leukemia (PML) gene was first described in the early 1990s at the point of chromosomal translocation t (15, 17), where it was found to encode an oncogenic chimeric protein emerging from the fusion of PML and the retinoic acid receptor alpha (RAR-α) in patients with acute promyelocytic leukemia (APL). The PML-RAR chimeric protein prevents the differentiation of bone marrow progenitor cells, sustaining their self-renewal capacity and preventing their apoptotic process, leading to leukemogenesis[3,4]. PML protein is the key component of PML-NBs, which are nuclear membrane-less compartments self-assembled through the RBCC motif interactions. By interacting and/or participating in the post-translational modifications of various nuclear proteins, PML-NBs regulate a variety of cellular processes such as apoptosis, proteolysis, cellular aging, cell self-renewal

capacity, DNA damage response, telomere stability, gene expression and chromatin/epigenetic states[5,6]. For example PML is highly expressed during murine mammary gland development, it's barely detectable during pregnancy and lactation and it's necessary for lineage commitment of bi-potent luminal progenitor cells[7]. Moreover PML is essential for sustaining naïve pluripotent state in mouse embryonic stem cells[8].The role of PML in neoplasias seems to be complex. PML protein is lost in human cancers of various histologic origins, including breast cancer[9]. Various reports support a tumor suppressive role for PML[10]. Using a doxycycline inducible overexpression of PMLIV in the triple negative (TNBC) MDAMB231 cell line, we found a strong inhibition of cell proliferation and tumor sphere formation ability[11]. Other studies point to a pro-survival role of PML in non-tumorigenic or tumorigenic breast cell lines and find that high PML levels correlate with poor prognosis in a breast cancer cohort[12]. Similarly, high PML expression in chronic myeloid leukemia maintains hematopoietic stem cells and PML ablation leads to an increase of their initial cycling activity that eventually leads to their eradication[13]. These studies suggest that PML may have divergent cells effects not only in different cell contexts but also in different temporal windows i.e. short vs long-term effects.

Here we show that constitutive PML loss enhances cell migration *in vitro* & metastatic aggressiveness *in vivo* of TNBC cells. Transcriptional profiling showed enrichment in cell cycle and adhesion related gene categories deregulated by PML ablation. Moreover cells derived from *in vivo* primary tumors or lung metastasis stably maintain an *in vivo* aggressive phenotype and transcriptionally resemble the earlier described lung metastasis signature (LMS)[14] . We found that PML loss deregulates the hypoxia signaling pathway and enhances *in vivo* tumor angiogenesis. In addition we found that PML interacts and functionally affects the activity of EMT mediators, such as TWIST2. Thus, PML may impede the aggressive EMT-metastatic behavior of TNBC cells.

MATERIALS AND METHODS

Plasmids, DNA, and siRNA transfections

Plasmids with PMLIV, PMLIII and PMLI isoforms have been previously described[15]. For immunoprecipitation and localization experiments the PMLIV, PMLIII and PMLI isoforms were fused to to the mRED vector (Clontech, Mountain View, CA, USA). TWIST1, TWIST2, SNAIL1 (Addgene #16225[16]) and SLUG (Addgene #25696) were fused to GFP-C (Clontech). mCherry LEGO-C2 was provided by Dr. K. Weber. The 5xHREVEGFLuc reporter was provided by Dr. S. Simos. Transient transfections were performed using the calcium phosphate DNA precipitation method or Lipofectamine 2000 (Thermo Fisher Scientific, Waltham, MA, USA) according to the manufacturer's instructions. The lentivirus production and infection protocol have been previously described in detail[17].

Cell culture and generation of stable cell lines

Human breast cancer cell lines MDAMB231, MCF7 and HEK293T were provided from ATCC and cultured in DMEM, 10% FBS and gentamycin 1%, 5% CO2 and 37°C. Cell lines were authenticated by STR analysis cell and were periodically screened for being mycoplasma negative. For the generation of stable, knock down cell lines, cells were infected by puromycin expressing lentiviral vectors carrying the relevant sh RNA sequences, followed by drug selection. The shPML short-hairpin RNA sequences that we used were: Sh0:5'-AGATGCAGCTGTATCCAAG-3'[18], Sh1: 5'-GCTGTATCCAAGAAAGCCA-3', sh2: 5-CCAACAACATCTTCTGCTCC-3' were cloned into the lentiviral vector pLKO.1 (Addgene #8453)[19]. Knockdown (KD) was evaluated by western blot and/or mRNA analysis using suitable primers.

Tumor Sphere Forming assay

For tumorsphere forming assays cells were cultured in DMEM-F12 1:1 (Gibco, Waltham, Massachusetts, USA) containing B27 (1:50), bFGF (20ng/ml), EGF (20ng/ml) and 0.2% methylcellulose at 1000 cells/ml using in ultra-low attachment plates. After 8 days, spheres of > 70µm size were enumerated and if required were dispersed by Accutase and cells were counted for next passage.

RNA extraction and qRT-PCR

Total RNA extraction was performed using Nucleozol (Macherey-Nagel, Germany). Next, 2µg RNA was used to generate library cDNAs using the enzyme M-MuLV Reverse Transcriptase (New England, Biolabs, USA) together with an RNase inhibitor (New England, Biolabs, USA) according to the manufacturer's protocol. The relative abundance of each gene transcript was measured by qRT-PCR using the dye SYBR Green I (Invitrogen, Waltham, Massachusetts, USA). Relative mRNA expression was calculated after normalization against β-actin or GAPDH levels. Set of primers used for qRT-PCR are listed below in Table1.

Table 1: Primers set used for quantitatve RT-PCR	
PML F: 5'- GATGGCTTCGACGAGTTCAA-3'	R: 5'- GGGCTGGCTTCCTTGGATAC-3'
ACTIN B F: 5' CCTGTACGCCAACACAGTG 3'	R: 5'-ATACTCCTGCTTGCTGATCC 3'
GAPDH F:5'- CAGTCAGCCGCATCTTCTTT-3'	R: 5'- ACCAGAGTTAAAAGCAGCCC-3'
TOP2A F: 5'-TCAAACGGAATGACAAGCGA-3'	R: 5'-ATGGGCTGCAAGAGGTTTAG-3'
PCNA F: 5'-TTTCCTGTGCAAAAGACGGA-3'	R: 5'-CCGTTGAAGAGAGTGGAGTGG-3'
p21 F: 5'-CCGCTCTACATCTTCTGCCTTAGTC-3'	R: 5'-AACCTCTCATTCAACCGCCTAGTT-3'
HDAC9 F: 5'-GGTGGACAGTGACACCATTT-3'	R: 5'-TGGATTCTTCAGCGTGATGG-3'
MMP1 F:5'-GGGCTTTGATGTACCCTAGC-3'	R:5'-ACTTCCGGGTAGAAGGGATT-3'
CD24 F:5'-TGCTCCTACCCACGCAGATT-3'	R:5'-GGCCAACCCAGAGTTGGAA-3'
EpCAM F:5'-TTCTAAGAAAATGGACCTGACA-3'	R:5'-TTCCCTATGCATCTCACCCA-3'
CDH1 F:5'-CTCACACACCCCCTGTTGGT-3'	R:5'-GTGAATTCGGGCTTGTTGTC-3'
VEGFα F:5'-CAGAATCATCACGAAGTGGTG-3'	R:5'-GAAGATGTCCACCAGGGTC-3

CD49f (ITGA6) F: 5’-TCATGGATCTGCAAATGGAA-3’	R: 5’- AGGGAACCAACAGCAACATC-3’
IL6ST(gp130) F: 5’- CGAAGCTGTCTTAGAGTGGG-3’	R: 5’- AAGCAAACAGGCACGACTAT-3’
PIM1 F: 5’-CGAGCATACGAAGAGATCA-3’	R: 5’-TCGGGCATCTGACAAGAGA-3’
IL6 F: 5’-ACTGGCAGAAAACAACCTA-3’	R: 5’-CAGGGGTGGTTATTGCATCT-3’
TGFβR2 F: 5’-TGCCCCAGCTGTAATAGGACC-3’	R: 5’-CCATACAGCCACACAGACTT-3’
EZH2 F: 5’- TCCTTTTCATGCAACACCCA-3’	R: 5’- TTTCAGTCCCTGCTTCCCTA-3’
SLIT2 F: 5’- ACCAGTCATTTATGGCTCCTTC-3’	R: 5’- TCAGAGAGCGTAGTCCTTGG-3’
ISL1 F: 5’- GGCAATCAGATTCACGATCAG-3’	R: 5’- GCGCATTTGATCCCGTACAA-3’
XIST F: 5’- CACGTGTATGTCTCCCAGTG	R: 5'- GTGAGGCACCAATACAGAGG-3’
ID1 F: 5’- AAACGTGCTGCTCTACGACA-3’	R: 5'- GAGAATCTCCACCTTGCTCAC-3’
FASCIN F: 5’- CAGCGGCCTCTCGTCTA-3’	R: 5'- AGATCTGCTTCTTCTTCAGGC-3’

RNA sequencing

Total RNA was isolated from control cells and PML KD using TRIzol (Invitrogen). For the MDAMB231 samples, the mRNA 3'-UTR sequence method was used to create libraries with the QuantSeq 3'mRNA-Seq Library Prep Kit for Ion Torrent-Cat #012. And the sequencing was done with Ion S5, with Ion 540 Reagents. NEBNext Ultra II Directional RNA Library Prep Kit for Illumina-E7760 and NEBNext Poly (A) mRNA Magnetic Isolation Module-E7490 were used for libraries for complete RNA sequencing of MCF7 cells. Sequencing was performed on the NextSeq 500 Illumina with FlowCell High 1x75. HISAT2 version 2.1 (genome mapper)

Analysis of differentially expressed genes

Differential gene expression analysis was performed with MetaseqR. The functional analysis was performed using the web tool gProfileR[20]

Western-Blot Analysis

Whole cell lysates were prepared using RIPA cell lysis buffer (25 mm Tris pH 7.6, 150 mm NaCl, 1% NP-40, 1% deoxycholate, 0.1% SDS, 1 mm PMSF) containing protease inhibitor cocktail (Complete; Sigma), and protein concentration was determined by Bradford assay. Equal amounts of cell lysates were subjected to SDS/PAGE, followed by immunoblotting. The primary antibodies used for WB are listed below in Table 2.

Table 2: Antibodies used for Western blot analysis	
PML	sc-377340 Santa Cruz, Dallas, Texas, USA
β-ACTIN	sc-47778, Santa Cruz
GAPDH	sc-32233, Santa Cruz
p21	sc-397, Santa Cruz
STAT3	sc-8019, Santa Cruz
p-STAT3	9145S, Cell signaling, Danvers, Massachusetts, USA
VIMENTIN	5741S, Cell signaling
E-CADHERIN	3195S, Cell signaling
GFP	sc-9996, Santa Cruz
ERa	M7047, DAKO, Denmark

Protein immunoprecipitation (Immunoprecipitation-IP)

Immunoprecipitation of protein complexes was performed, using HEK293T cell extracts following overexpression of specific proteins for possible interaction and prepared by RIPA cell lysis buffer as described above. 200µg of protein extracts were incubated with primary antibody overnight at 4 °C. The following day, 20 µL of protein G beads was added to each sample after washing with IP buffer (25 mm Tris/HCl pH 7.6, 150 mm NaCl), and reactions were incubated at 4 °C for three additional hours. Non-specific proteins were washed away three times with NETN buffer (10 mm Tris/HCl pH 8.0, 250 mm NaCl, 5 mm EDTA, 0.5% NP-40, 1 mm PMSF). SDS sample buffer was added, and the samples were boiled prior to SDS/PAGE analysis. Input lanes represent 10% of the lysate used for the IP.

FACs analysis

Flow cytometry was used to evaluate CD24 and CD44 surface expression (FACs calibour by Becton Dickinson(BD) (Franklin Lakes, New Jersey, USA). The cells were detached with trypsin-EDTA and following centrifugation were suspended in PBS-2% FCS-0.1% NaN3 with specific antibodies of isotype controls.

Cell migration assay

For migration assays, cells were seeded into Millicell, Cell culture 8µm inserts (Merck KGaA, Germany) in FBS-free medium overlaying the lower compartment filled with FBs-containing media. The next day, the upper side cells were scraped away and the insert was fixed with 70% ethanol, stained with crystal violet (Merck) and counted under a microscope. The percentage of cells that has passed through the

membrane in relation to the total number of cells seeded on the transwell is indicative of the migrating capacity of the cells.

Immunostaining and microscopy

Cells for immunostaining were cultured on 8-well chamber, removable (80841, Ibidi GmbH, Germany) and fixed in buffered 4% PFA / 1XPBS for 5 minutes at room temperature, permeated with 0.5% Triton X-100/1XPBS for 5 minutes and rinsed repeatedly with 1XPBS. The samples were then incubated with 1% BSA/1XPBS for 1 hour before incubation with primary antibodies overnight or 1 hour. After washing with PBS, secondary antibody was added to the samples for one hour. The secondary antibody was washed again three times with PBS and the cell nuclei were then counter stained with DAPI (Merck). Epifluorescence microscopy was done in an inverted Olympus IX70 and Confocal microscopy was done in a Zeiss Axioscope 2 Plus microscope equipped with a Bio-Rad Radiance 2100 laser scanning system and Lasersharp 2000 imaging software and a Leica SP8 inverted focus microscope and analyzed with the Leica Application Suite (Las, Leica, Germany) software. Autopsied animals were examined under a Leica M205FA fluorescent stereomicroscope, carrying a Leica DFC310FX camera and analysed with Leica Application Suite (Las) software.

Immunohistochemistry in paraffin sections

Tissues isolated from experimental animals were fixed with 10% formalin (Merck) and kept overnight at 4° C. They were then washed 3 times with sterile PBS and placed in 70% sterile ethanol (analytical grade). They were then placed in a sequential dehydration and paraffinization machine and finally the tissues were placed in paraffin to be cut into a microtome and stained with hematoxylin-eosin as described in a previous study[21]. If required, sections were stained with antibody CD31 (AbCAM, Cambridge,UK) and stained area was measured with ImageJ as percentage of Microvessel density.

In vivo experiments on experimental animals

Tumor Xenografting was done in NOD-scid IL2Rgammanull (NSG) mice. In the case of MCF7 cells, β-estradiol (8μg / ml) was added to the water and was being replaced every 5 days until termination of the experiment. Tumor volume was estimated using the formula $V = ½ (Length \times Width^2)$[22]. To better monitor the engrafted tumour cells, control and KD PML cells were previously modified to express the red fluorescent mCherry protein. Equal cell numbers from either group were injected subcutaneously into NSG mice and measurements from the growing primary tumors were taken every four days. When tumors reached 1200mm^3 in size, mice were sacrificed.

Approval of animal experiments

All procedures were conducted according to Greek national legislations and institutional policies following approval by the FORTH ethical committee. NSG mice were purchased from Jackson Laboratory (Bar Harbor, Maine, USA) and were maintained and bred at the Institute of Molecular Biology and Biotechnology (IMBB) animal facility following the institutional guidelines based on the Greek ethical committee of animal experimentation. Current procedures were approved by the General Directorate of Veterinary Services, Region of Crete (license number: 93304).

Statistical analysis

The statistical study was performed with Microsoft EXCEL software, XLSTAT and Graphpad Prism. Values were presented as the mean + SD.

RESULTS

Silencing of PML affects tumor cell morphology and physiology

To dissect the role of PML in breast cancer we initially employed a doxycycline inducible shRNA approach that resulted in 50-55% reduction of the various PML isoforms. Thus we switched to a constitutive knock down approach by testing three different shRNAs for PML silencing in MDAMB231 and MCF7 cells. Knock down (KD) efficiency was verified by qRTPCR (not shown), immunostaining and western blotting using an antibody against a region common to all PML isoforms (Fig.1A) and cell pools with more than 80% PML protein reduction were chosen for further experimentation.

Fig.1

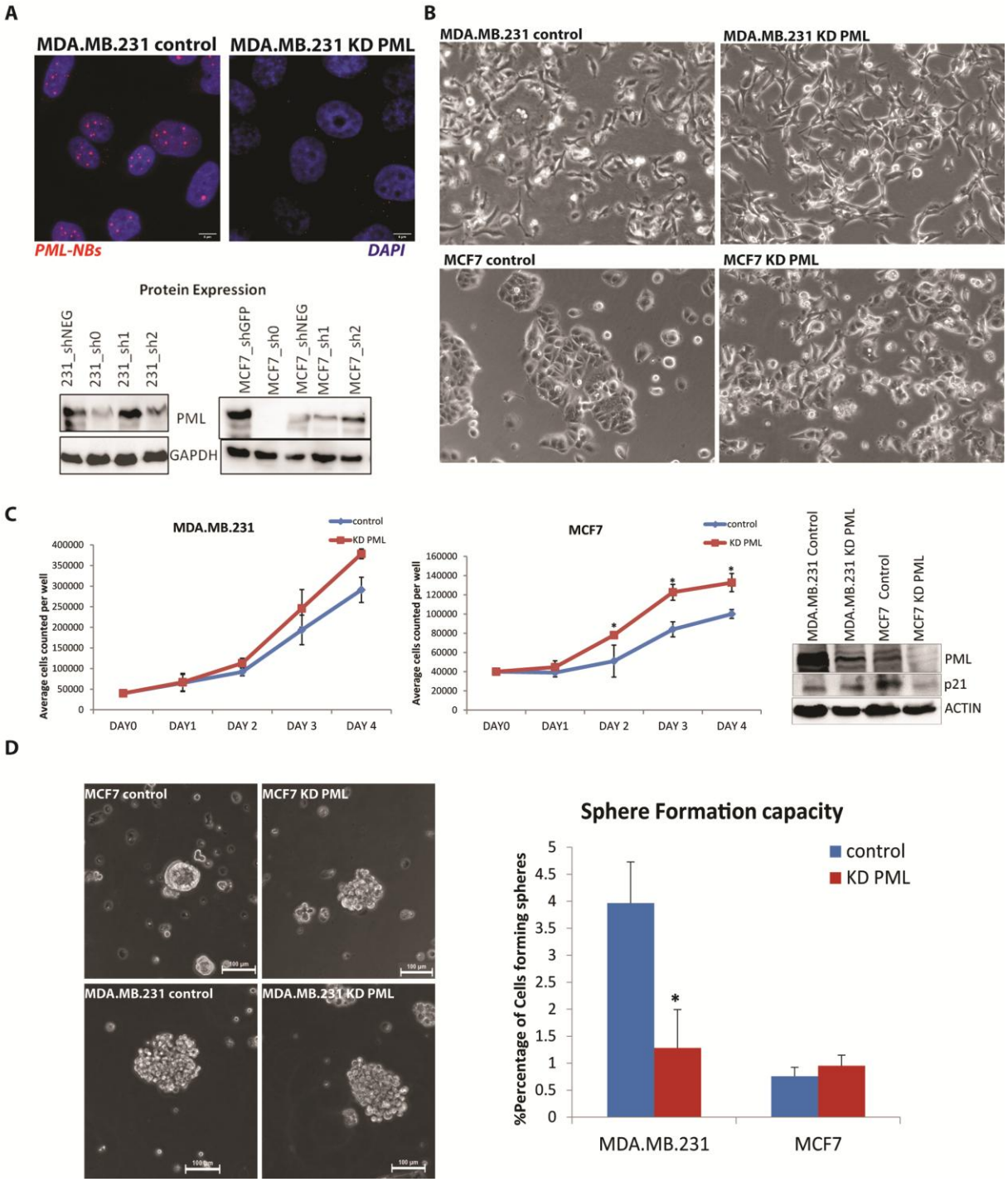

Figure 1 (A) Upper: Confocal microscopy of PML Immunostaining (red nuclear speckles) in control and PML–KD MDAMB231 cells counterstained by DAPI (blue). Lower: Immunoblotting for PML protein expression of puromycin selected pools of MCF7 and MDAMB231 using a sh-scrabbled control and 3 different sh-PML (sh0, sh1, sh2) targeting sequences. All further experiments were performed using the most efficient sh0 sequence. (B) Phase contrast microscopy of MDAMB231 KD PML & MCF7 KD PML compared to sh-scrabbled controls. (C) Cell growth of control and PML KD, MDAMB231 (left) and MCF7 (middle) cells. Results show mean ±SD from one out of three independent triplicate experiments with similar results.

t-test, *p-value≤0.05. Right: Immunoblot of p21 protein levels (CDKN1A) in control and PML KD cell lines. (D) Morphology of 3D tumorspheres of control or PML KD, MCF7 and MDAMB231 (left) and tumor sphere forming efficiency (right). Shown is mean ±SD of % sphere forming cells from one of at least two quadruplicate experiments with similar results. t-test * p-value ≤0.05

Microscopic examination of control and KD cells showed moderate changes of cell morphology in sparse cultures, towards a more spindle–like shape of MDAMB231 (Fig.1B). Similarly, MCF7 acquired a less tight epithelial cell-to-cell adhesion pattern. PML silencing slightly increased the proliferation of MDAMB231 and to a larger extend MCF7 in agreement with reduced expression of the cyclin kinase inhibitor p21 protein (Fig.1C). We next tested the impact of PML ablation on cells grown in 3D as tumour spheres. Parental MCF7 and MDAMB231 formed compact-round and grape-like spheres respectively[23]. The MCF7-PML KD spheres assumed a more loose morphology that tends to resemble those of MDAMB231 cells (Fig.1D). Most importantly the sphere forming efficiency of MDAMB231 – PML KD cells, but not that of MCF7 cells was reduced to about 30% of the control cells (Fig.1D).

We have shown previously that PML is essential for maintaining the epithelial characteristics of naïve mouse embryonic stem cells[8]. The MDAMB231 cell line has mesenchymal characteristics, expressing high levels of VIMENTIN compared to MCF7 (Fig.2A/middle). Conversely, MCF7 express high levels of the epithelial marker CDH1 as compared to MDA-MD-231 cells. Following PML KD we observed a decrease of CDH1 RNA in both MDA–MB-231 and MCF7 cells (Fig 2A/left). At the protein level, the Vimentin expression was slightly increased in the former whereas the CDH1 was decreased in the latter cells (Fig.2A/right). MDAMB231 cells express high levels of the mesenchymal marker CD44 and intermediate levels of the epithelial marker CD24, a phenotype early on linked to high tumour initiating (or cancer stem cell) ability of patients-derived breast cancer xenografts[24]. Flow cytometry analysis for those surface markers showed that PML loss minimally affected CD24 or CD44 expression in MCF7 cells. However, PMLKD in MDAMB231, led to a reduction of the $CD24^+$ population (Fig.2B) and lower CD24 RNA expression (Fig.6D). To further assess the epithelial/mesenchymal cell properties we used an *in vitro* transwell assay, and found that the absence of PML led to increased migration capacity of MDAMB231 and to a lesser extend MCF7 cells (Fig.2C). Moreover the amount of phosphorylated STAT3 protein, known to correlate with TNBC aggressive behaviour[25,26], was increased (Fig.2D).

Thus, PML loss seems to intensify the existing mesenchymal phenotype while reducing the epithelial phenotype of MDAMB231 cells, whereas in MCF7 cells, leads to a decrease of the CDH1 epithelial marker without inducing mesenchymal marker expression. Because epithelial-mesenchymal transition (EMT) transcription factors (EMT-TFs) are mediators of the above phenotypic changes, we measured protein levels of a key EMT factor TWIST2 and observed that PML loss in MDAMB231 cells led to a significant increase at the protein level (Fig.6E).

Fig.2

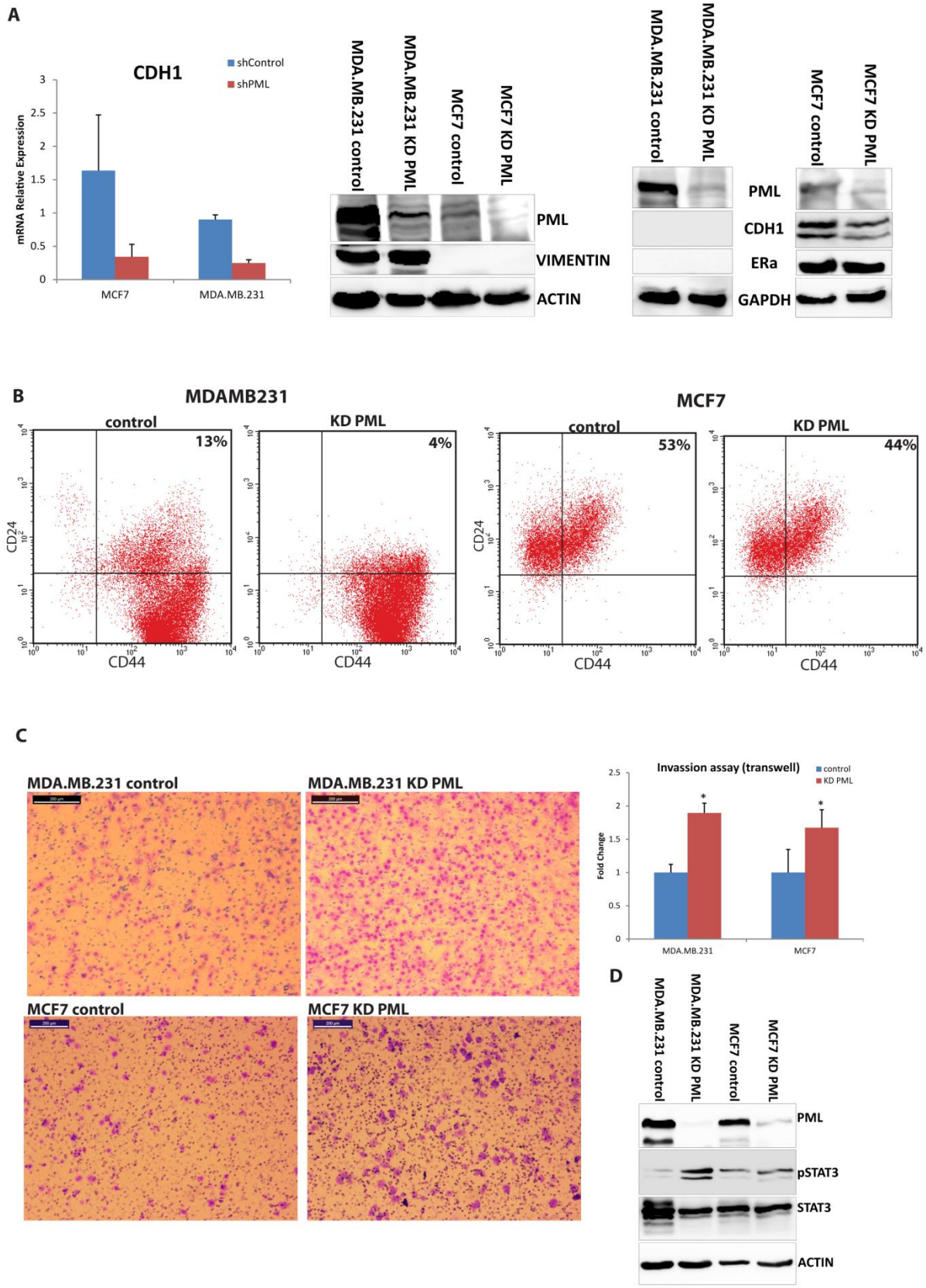
A
CDH1
shControl
shPML
mRNA Relative Expression
MCF7
MDA.MB.231
MDA.MB.231 control
MDA.MB.231 KD PML
MCF7 control
MCF7 KD PML
PML
VIMENTIN
ACTIN
CDH1
ERa
GAPDH
B
MDAMB231
MCF7
control
KD PML
13%
4%
53%
44%
CD24
CD44
C
MDA.MB.231 control
MDA.MB.231 KD PML
MCF7 control
MCF7 KD PML
Invassion assay (transwell)
control
KD PML
Fold Change
D
pSTAT3
STAT3

Figure 2 (A) qRT-PCR of MDAMB231 and MCF7, control and PML -KD cells of CDH1 expression (left). Results are mean ±SD from a triplicate experiment. Protein expression of a mesenchymal marker (Vimentin) (middle) and an epithelial (CDH1) (right). Actin and GAPDH are loading controls. (B) Flow cytometry for CD44 and CD24 surface expression in control and PML KD MDAMB231 (left panels) & MCF7 (right panels) cells. (C) Microscopy of migrated, MDAMB231 and MCF7 control or PML KD cells (Left panels). Quantitation (%) of crossing cells ±SD mean of one triplicate experiment (Right). t-test *p-value≤0.05. (D) Immunoblot for pSTAT3 protein (Tyr-705) and total STAT3.

To further study the relationship of PML and EMT factors, PML-mCherry fusions and EMT factor-GFP fusions of TWIST1,TWIST2, SNAIL1 AND SLUG (SNAIL2) were co-expressed in HEK293T cells. PMLIV strongly co-localize with all EMT factors especially with TWIST2 and SLUG (Fig.3A), whereas PML III or PML I did not (Suppl. Fig S1). A strong physical interaction of EMT factors and PML was further confirmed by co-immunoprecipitations. Figure 3B shows results from a representative co-IP using PMLIV. To define the region involved in the protein–protein interaction, we expressed TWIST2 truncations along with PMLIV followed by confocal microscopy and co-immunoprecipitation. Confocal results showed localization with the central region of TWIST2 that includes the bHLH. Indeed the HLH region alone (aa64 to aa124) showed a strong co-IP signal whereas the N- or C-terminal parts had minimal or no interaction ability (Suppl. Fig S2).

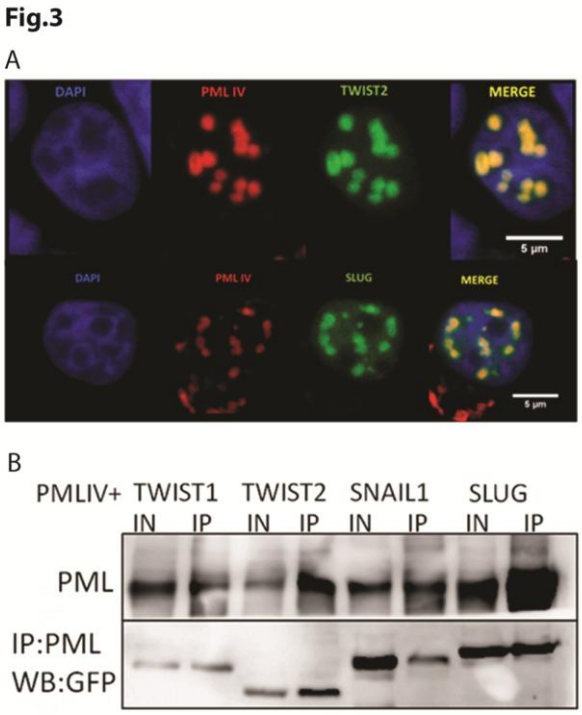

Figure 3 (A) Confocal images of co-localisation between PML isoform IV (fused to mRED) and TWIST2 or SLUG (fused to GFP). (B) Co-immunoprecipitation of PML with TWIST 1, TWIST2, SNAIL1 AND SLUG following co-expression in HEK293T cells. IN: input; IP: immunoprecipitation.

Changes in gene expression induced by PML ablation in breast cancer cells

To correlate the above changes in cell behaviour with potential effects of PML loss in gene expression, we performed transcriptomic analyses of control and PML KD cell lines. Specifically, silencing of PML deregulated about 600 genes at the 1.5 fold cut-off in MDAMB231 cells. Upregulated genes were enriched in cell cycle and cell division, whereas down- regulated genes showed enrichment in cell adhesion functions, Epithelial Mesenchymal Transition (EMT) and microRNAs that target tumour suppressors (Fig.4). A similar analysis of control and PML KD MCF7 cells identified 736 down- and 256 up-regulated genes. Upregulated genes were enriched in differentiation, morphogenesis, locomotion, and cell adhesion terms that involve NFKB1, RELA, and HIF1A factors while down regulated genes involve ECM organisation and cytokine signalling.Validation of deregulated expression for a number of those genes was done by qRT-PCR analysis (Suppl. Fig S3).

Comparisons of the two cell types showed little overlap in deregulated genes indicating a cellular context-specific response to PML loss. Common GO terms were related to stress response and developmental processes.

Fig.4

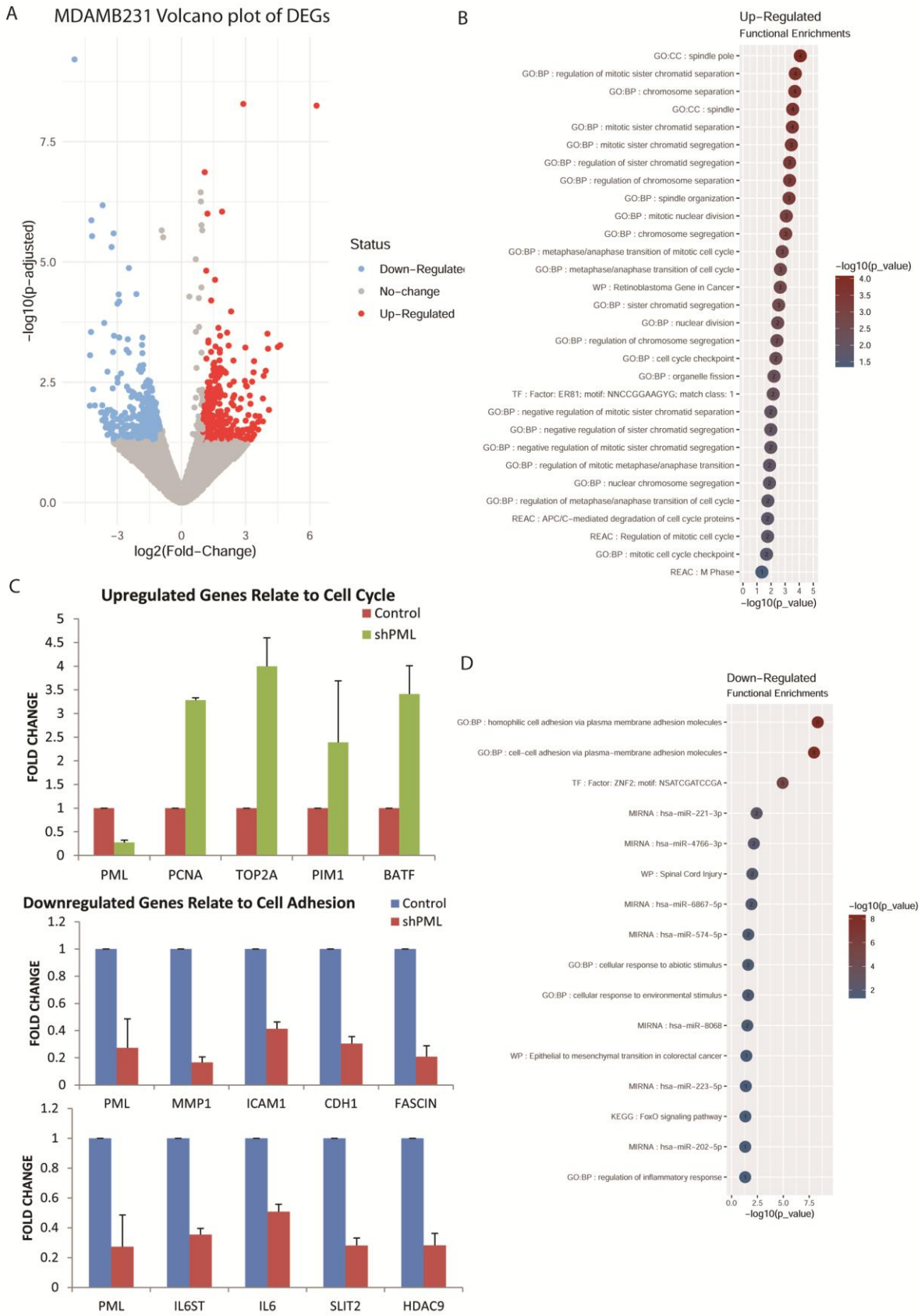
A
MDAMB231 Volcano plot of DEGs
−log10(p−adjusted)
log2(Fold−Change)
Status
Down−Regulated
No−change
Up−Regulated
B
Up−Regulated
Functional Enrichments
GO:CC : spindle pole
GO:BP : regulation of mitotic sister chromatid separation
GO:BP : chromosome separation
GO:CC : spindle
GO:BP : mitotic sister chromatid separation
GO:BP : mitotic sister chromatid segregation
GO:BP : regulation of sister chromatid segregation
GO:BP : regulation of chromosome separation
GO:BP : spindle organization
GO:BP : mitotic nuclear division
GO:BP : chromosome segregation
GO:BP : metaphase/anaphase transition of mitotic cell cycle
GO:BP : metaphase/anaphase transition of cell cycle
WP : Retinoblastoma Gene in Cancer
GO:BP : sister chromatid segregation
GO:BP : nuclear division
GO:BP : regulation of chromosome segregation
GO:BP : cell cycle checkpoint
GO:BP : organelle fission
TF : Factor: ER81; motif: NNCCGGAAGYG; match class: 1
GO:BP : negative regulation of mitotic sister chromatid separation
GO:BP : negative regulation of sister chromatid segregation
GO:BP : negative regulation of mitotic sister chromatid segregation
GO:BP : regulation of mitotic metaphase/anaphase transition
GO:BP : nuclear chromosome segregation
GO:BP : regulation of metaphase/anaphase transition of cell cycle
REAC : APC/C−mediated degradation of cell cycle proteins
REAC : Regulation of mitotic cell cycle
GO:BP : mitotic cell cycle checkpoint
REAC : M Phase
−log10(p_value)
C
Upregulated Genes Relate to Cell Cycle
Control
shPML
FOLD CHANGE
PML
PCNA
TOP2A
PIM1
BATF
Downregulated Genes Relate to Cell Adhesion
Control
shPML
FOLD CHANGE
PML
MMP1
ICAM1
CDH1
FASCIN
FOLD CHANGE
PML
IL6ST
IL6
SLIT2
HDAC9
D
Down−Regulated
Functional Enrichments
GO:BP : homophilic cell adhesion via plasma membrane adhesion molecules
GO:BP : cell−cell adhesion via plasma−membrane adhesion molecules
TF : Factor: ZNF2; motif: NSATCGATCCGA
MIRNA : hsa−miR−221−3p
MIRNA : hsa−miR−4766−3p
WP : Spinal Cord Injury
MIRNA : hsa−miR−6867−5p
MIRNA : hsa−miR−574−5p
GO:BP : cellular response to abiotic stimulus
GO:BP : cellular response to environmental stimulus
MIRNA : hsa−miR−8068
WP : Epithelial to mesenchymal transition in colorectal cancer
MIRNA : hsa−miR−223−5p
KEGG : FoxO signaling pathway
MIRNA : hsa−miR−202−5p
GO:BP : regulation of inflammatory response
−log10(p_value)

Figure 4 (A) Volcano plot of differentially expressed genes in MDAMB231 KD PML, compared to control cells with p-value≤ 0.05, and log2 (FC)≥ 1. (B) Top enriched cellular processes of upregulated or down regulated (D) genes by PML loss in MDAMB231 cells. (C) Genes validated by qRT-PCR. Results are mean ±SD from a triplicate experiment.

PML affects growth and hypoxic response of tumors derived from MDAMB231 xenografted cells.

To study and correlate the above results with the *in vivo* tumor growth of PML-silenced cells, we performed engraftment in NSG mice. PML loss led to an increase of the tumour growth rate in MDAMB231 cells, but not MCF7 cells (Fig.5A). Histology of primary MDAMB231 KD PML tumour sites showed reduced necrosis relative to control group (Fig.5B). To test whether reduced necrosis might be due to enhanced vascularization we used anti CD31 antibody staining in sections of primary site tumors. PML KD tumors showed significantly higher microvessel density relative to the control group (Fig.5C). To further study these cells after their *in vivo* passage, we readapted tumor tissue back into cell culture and developed more than 16 lines from primary or metastastic sites . To examine whether PML loss directly affects hypoxia-vascular response of MDAMB231 cells, we measured luciferase activity of a hypoxia reporter that carries 5 copies of the VEGF-α hypoxia response element. Transient transfections showed higher luciferase activity in the PML KD-MDA –MB-231 cells. (Fig.5D). Western blot analysis of xenograft cell lines from primary tumor or lung metastatic showed that PML KD had higher HIF protein levels in normoxia , whereas the parental cell lines had no significant differencies. (Fig.5E). Expression of VEGF-α, a target of HIF1a and a main angiogenic factor, showed an increase in all the KD PML groups (Fig.5F). Taken together these results suggest that PML loss facilitated in the acquisition of a hypoxic phenotype that is intensified upon in vivo cell growth

Fig 5

A

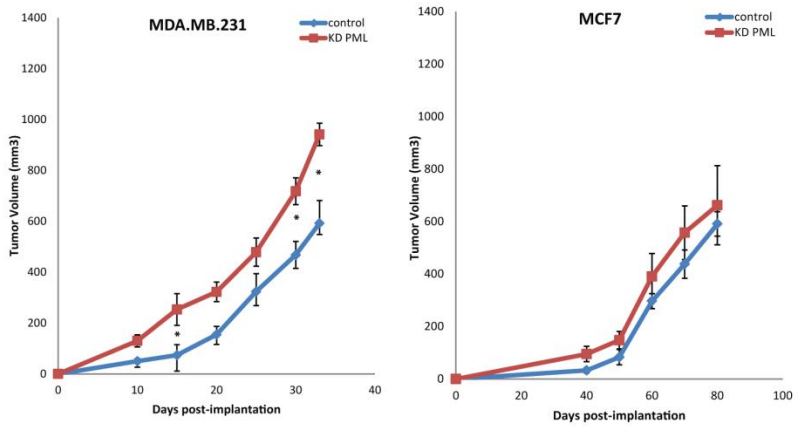
MDA.MB.231
control
KD PML
Tumor Volume (mm3)
Days post-implantation
MCF7
control
KD PML
Tumor Volume (mm3)
Days post-implantation

B

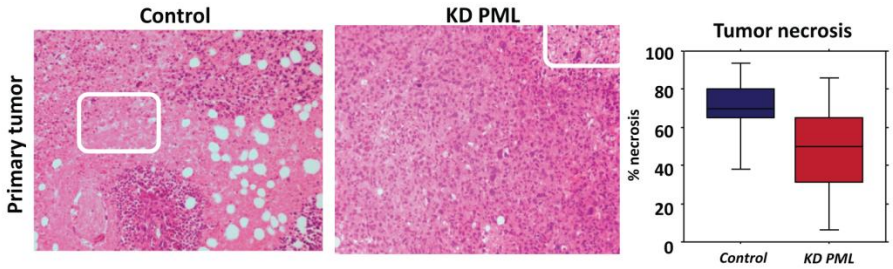
Control
KD PML
Primary tumor
Tumor necrosis
% necrosis
Control
KD PML

C

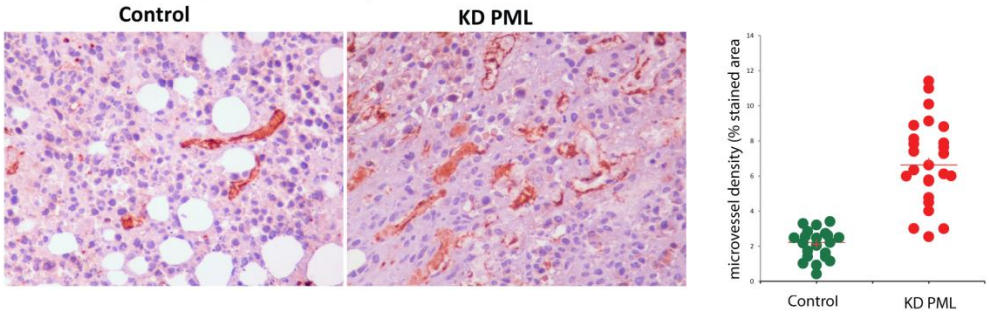
Control
KD PML
microvessel density (% stained area
Control
KD PML

D

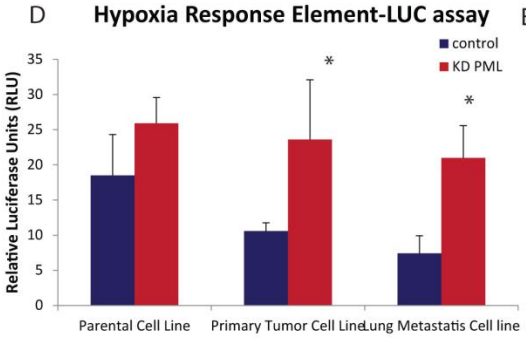
Hypoxia Response Element-LUC assay
control
KD PML
Relative Luciferase Units (RLU)
Parental Cell Line
Primary Tumor Cell Line
Lung Metastatis Cell line

E

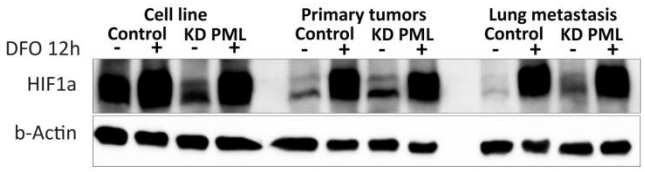
Cell line
Primary tumors
Lung metastasis
Control
KD PML
DFO 12h
HIF1a
b-Actin

F

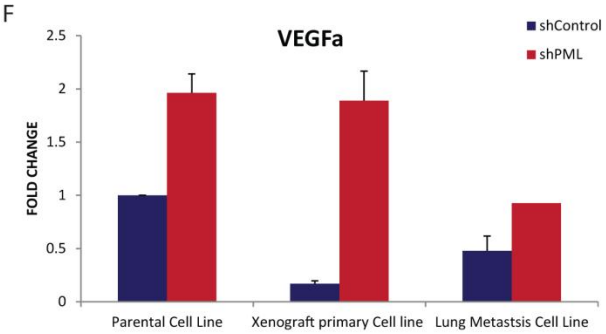
VEGFa
shControl
shPML
FOLD CHANGE
Parental Cell Line
Xenograft primary Cell line
Lung Metastsis Cell Line

Figure 5 (A) Tumor growth of MDAMB231 and MCF7, control (blue, n=7) & KD PML (red, n=7). Results show mean volume ±SD from one of two independent experiments with similar outcomes. *t-test p-value≤ 0.05. (B) Hematoxylin -Eosin at 100x magnification of primary MDAMB231 control & KD PML tumors (left). Rectangles indicate necrosis. Quantitation of primary tumor necrosis is presented by box plots of % necrotic area of primary tumors (n=7/group, Mann Whitney U,p-value ≤0.05) (right). (C) CD31 staining at 100x magnification of primary MDAMB231 control & KD PML tumors (left). Quantitation of primary tumor staining with CD31, indicative of angiogenesis (n=21 areas for control group and 25 areas for KD PML group/2-5 representative areas per tumor/5 tumors) (right), *t-test p-value ≤0.001). (D) HRE-LUC assay of control or PML KD parental cell lines, and primary tumor site or lung metastasis derived cell lines. Results are mean ±SD from one out of two triplicate experiments with similar outcomes. *t-test p-value≤ 0.05. (E) Immunoblot for HIF1a protein in parental and xenograft derived lines from primary or lung metastatic MDAMB231 cells with or without DFO (Desferrioxamine 100 μM) treatment for 12h. (F) Comparative expression of VEGF-α, a gene target of HIF1a, in parental or xenograft derived cell lines. Results are mean ±SD from a triplicate experiment.

The ablation of PML increased the metastatic ability of MDAMB231 cells.

Gross observation and stereomicroscopy of autopsied tumor bearing mice showed that all (7/7) the PML KD expressing, MDAMB231 tumours, had a more intense metastatic load relative to controls in all the organs examined. More specifically all PML KD mice had many more lung metastatic foci, 6/7 were positive for liver metastases, 4/7 showed metastases in the axillary glands and one (1/7) showed metastasis to the bone marrow (Fig.6A) compared with tumors from control mice. These were further confirmed and quantified by stereomicroscopy and histology of axillary lymph node, liver, kidney and lung samples. Of note, lung was the most extensively affected site observed (Fig.6B,C) with an estimated 10 fold higher metastatic load in the PML KD (Fig.7A). MCF7 control or PML KD tumors showed no significantly different growth rate and no metastasis were found in either group (Suppl. Fig. S5). All PML control and KD lines derived from tumor tissue retained differential expression of PML RNA, and protein, similar to their parental cell lines (Suppl. Fig S4). Interestingly,MDAMB231 PML KD cells or tumor –derived lines had increased TWIST2 protein expression (Fig.6E). In addition, they showed higher expression levels *of* recurrence-metastasis related markers, such as EpCAM[27] and CD49f[28] (Suppl. fig S4) and reduced epithelial CD24 levels (Fig.6D).Thus PML KD cells are enriched in mesenchymal markers and properties consistent with a high pro-metastatic phenotype.

Fig.6

A

Organ Metastatic Intensity (Autopsy and Stereoscopic Fluorescence Observation)				
Cell type	MDA.MB.231			
	control		KD PML	
Lung	2/6	+	7/7	+++
Liver	0/6		6/7	++
Axillary LN	1/6	+	4/7	++
Femoral Bone	0/6		1/7	+

B

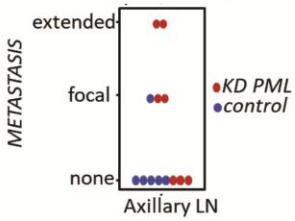

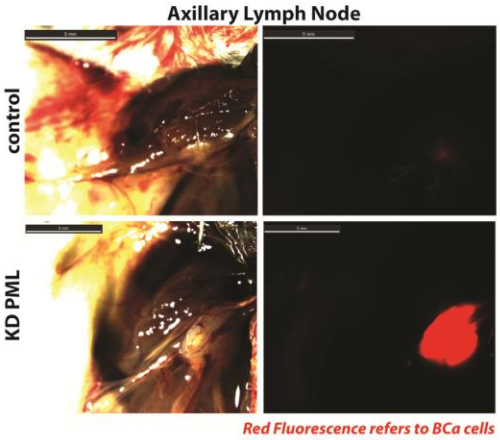

C

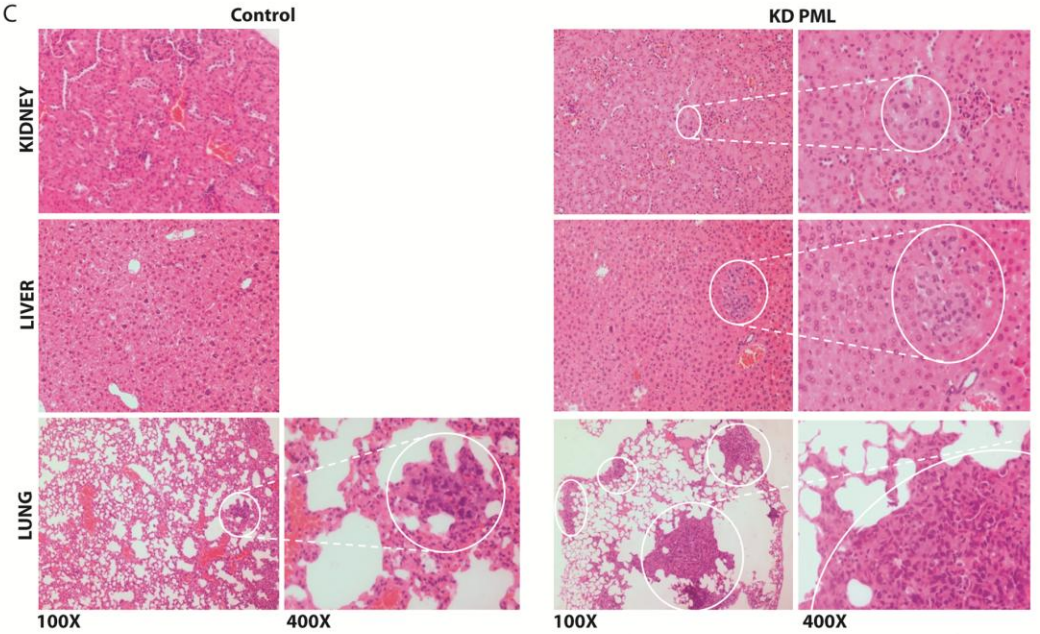

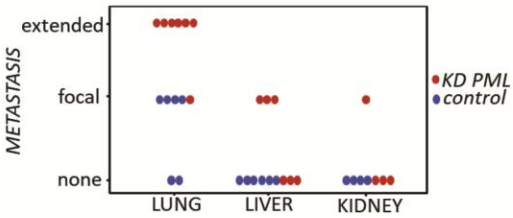

D

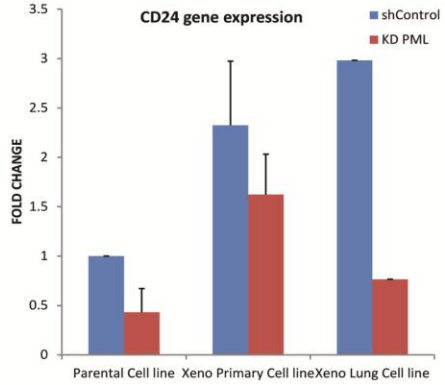

E

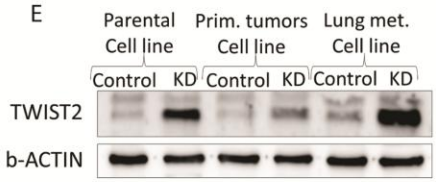

Figure 6 (A) Summary table of metastases in mice with MDAMB231 control & MDAMB231 KD PML cells and grading by stereoscopic observation as +:positive , ++:focal and +++:extensive. (B) ImageJ quantification of axillary gland metastasis by fluorescence stereomicroscopy ($\chi 2$ test p-value ≤ 0.05). Representative axillary gland metastasis imaged by visible or fluorescence stereomicroscopy (right). (C) Top: Representative Kidney, Liver and Lung histologies of control and PML -KD engrafted mice. Hematoxylin-Eosin staining at 100x and 400x magnifications. Encircled areas indicate metastatic foci. Bottom: Quantitation and $\chi 2$ test of metastatic load in control and PML-KD engrafted mice for Lung ($p=0.002$), Liver ($p=0.026$) and Kidney ($p=0.28$). (D) CD24 mRNA expression in parental and xenograft derived cell lines. (E) TWIST2 protein expression in parental and xenograft derived cell lines.

The increased lung metastatic ability of MDAMB231 PML KD derived tumour lines was maintained upon secondary xenografting (Fig.7C). By qRT-PCR analysis of characteristic lung metastasis signature genes, namely ID1 and FSCN1, using the original and tumor derived cell lines we found that PML KD derived cells had higher expression than their parental cell lines (Fig.7B). Because results of tumor sphere formation (TSF) ability seemed not to be in line with *in vivo* tumor growth, we chose to examine in more detail the TSF ability of parental and tumor derived MDA–MB-231 cell lines under normoxic or hypoxic conditions. Results from these experiments show that passage one (P1) PML KD from either parental or tumor derived lines, had a lower TSF ability (20-30%) than controls, under either normoxic or hypoxic (3% oxygen) conditions, although in the latter a general increase of TSF was found. However, during subsequent passages the TSF ability of PML KD cells increased whereas that of the control groups decreased. At P3, parental,primary tumor and lung derived PML KD cells exceeded their controls in pair wise comparisons (Fig.7D).

Fig.7

A

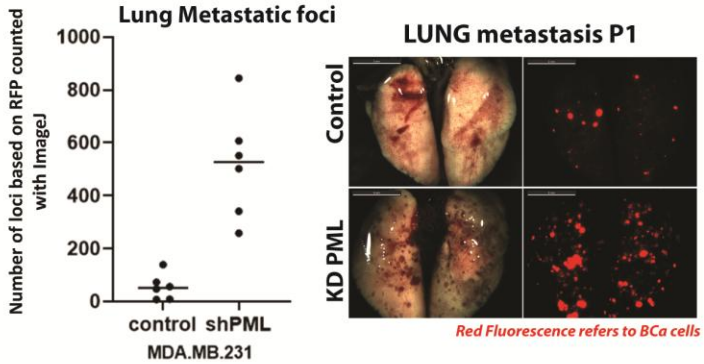
Lung Metastatic foci
Number of loci based on RFP counted with ImageJ
1000
800
600
400
200
0
control
shPML
MDA.MB.231
LUNG metastasis P1
Control
KD PML
Red Fluorescence refers to BCa cells

B

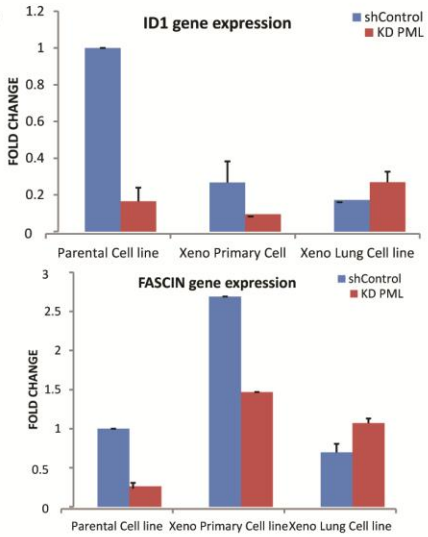
ID1 gene expression
shControl
KD PML
FOLD CHANGE
Parental Cell line
Xeno Primary Cell
Xeno Lung Cell line
FASCIN gene expression
shControl
KD PML
FOLD CHANGE
Parental Cell line
Xeno Primary Cell line
Xeno Lung Cell line

C

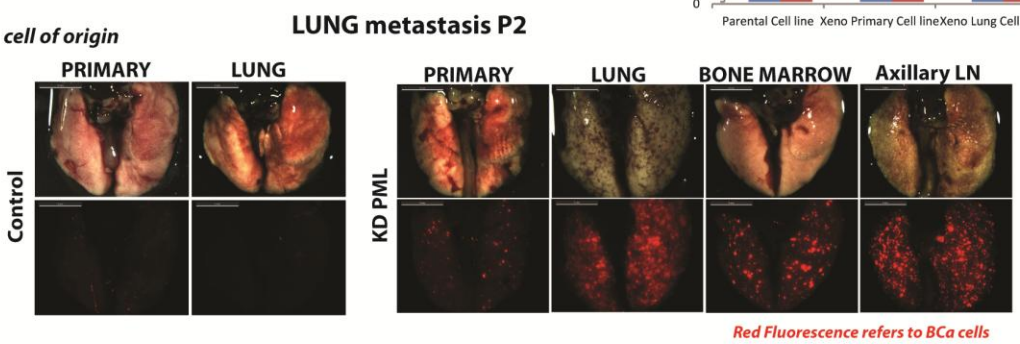
cell of origin
LUNG metastasis P2
PRIMARY
LUNG
PRIMARY
LUNG
BONE MARROW
Axillary LN
Control
KD PML
Red Fluorescence refers to BCa cells

D

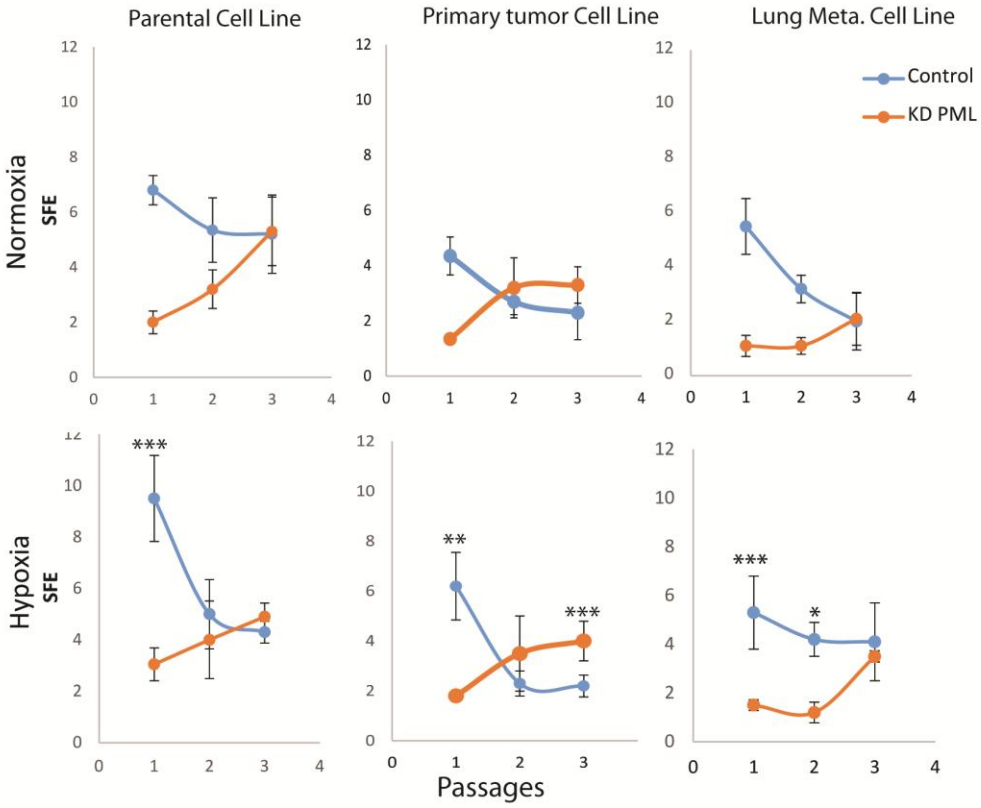
Parental Cell Line
Primary tumor Cell Line
Lung Meta. Cell Line
Control
KD PML
Normoxia
SFE
Hypoxia
SFE
***
**
***
***
*
Passages

Figure 7 (A) Assessment of Lung metastatic load of control and PML –KD engrafted mice by comparing (t-test, p-value≤0.05) total foci counts (left) and representative stereo microscopy image (middle). (B) Comparative expression of lung "metastasis signature"[14] (LMS) genes ID1 and FSCN1 in control and KD PML, parental and xenografts derived cell lines. Results are mean ±SD from a triplicate experiment. (C) Lung stereo microscopy from second passage (P2) of lung metastases following re-injection of first passage derived cells. (D) Percentage (%) of cells forming spheres (SFE), when cultured under normoxic or hypoxic conditions from parental and xenograft derived cell lines through sequential passaging P1, P2, P3. Results show mean SFE ±SD from one out of at least two experiments in quadruplicate. t-test *p-value≤0.05,p-value≤0.01***, p-value≤0.0001.**

DISCUSSION

To investigate the role of PML in breast cancer we produced Knock Down lines of the MDAMB231 and the MCF7 cells and studied their physiology and transcriptomic profiles. Our previous studies have shown that induced overexpression of PMLIV in MDAMB231 cells strongly inhibited cell proliferation and tumor sphere formation (TSF) ability[11]. While PML silencing of all PML isoforms in those cell types caused a slight increase of the cell growth rate in monolayer culture, yet their tumor sphere ability was compromised (25-30% of the control line) implying a role for PML in their maintenance of stem cell like properties. In addition, PML loss changed the MCF7 tumor spheres from their known smooth spherical morphology[23] to a more grape one, reflecting a change in the expression of cell–cell interacting proteins. The ablation of PML caused a shift in both cell line towards a more mesenchymal appearance that has been previously linked to increased cell invasiveness[29,30] and tumor recurrence or metastasis[31,32]. In accordance with this, PML deficient cells showed increased migration capacities. The increase in migration activity was more pronounced in MDA MB 231 cells and correlated with higher phosphorylated Stat3[33].

To correlate these changes with RNA expression profiles, we report here for the first time a transcriptomic analysis upon silencing of PML. The transcriptomic analysis reflected the differences in the physiology of these cell types. The ablation of PML in MDAMB231 cells caused the repression of genes related to cell adhesion and EMC. On the other hand, genes related to cell cycle, mitosis and cell division were upregulated. A similar analysis in MCF7 cells identified developmental –differentiation related genes to be upregulated and cytokine and extracellular matrix related genes to be repressed upon PML KD.

Together the phenotype and deregulated gene expression profile suggest that PML deficient MDAMB231 cells are expected to be more aggressive than their parental cells. This contrasts with the reduction in TSF that is thought to measure of tumor initiating cells (TICs) or cancer stem cell activity. To clarify this we xenografted control and PML KD cells in NSG mice and monitored their growth in the primary site and development of metastasis. PML KD did not affect significantly the local tumor growth or the non/low metastatic properties of MCF7 cells. However, MDAMB231 KD PML cells developed tumors faster when compared with the controls. This observation contradicts the *in vitro* TSF assay suggesting that the growth defect in PML loss can be reversed during *in vivo* tumor growth. Indeed, upon sequential tumor sphere passaging, PML KD cells showed a gradual increase of their TSF ability concomitant with a decrease of the control TSF. These results show that PML KD cells retain higher

long-term TSF ability especially when taken from primary tumor sites and/or hypoxic conditions in agreement with their higher *in vivo* tumor growth rate and metastasis. Taken together these results suggest that PML KD cells acquire higher TIC properties *in vivo* and show a more aggressive phenotype. Hypoxia seems to further intensify this process.

Tumors produced by MDAMB231 PML KD cells showed lower necrotic content suggesting higher vascular supply. In agreement with this, CD31 immunocytochemistry showed significant increase of microvessel density in PML KD primary tumors. Earlier work in a mouse PML KO model, has identified PML as an inhibitor of the mTOR-hypoxia-HIF1A signaling to control angiogenesis[34]. In agreement with this, cell lines generated generated from PML KD tumor xenografts showed higher activity of HIF1a and it's target VEGFα that correlates with a higher tumor angiogenic activity. This, in combination with an increase of mesenchymal-migratory properties of MDAMB231 PML KD cells may account for their higher *in vivo* aggressive properties. These results partly disagree, with the observations of Ponente et al.[35], Martin-Martin et al.[36] and Arreal et al.[37] that describe a pro-oncogenic role of PML in breast cancer. Although presently undetermined these differences may be caused by distinct MDAMB231 subline differences or the effect of long term and strong PML silencing in our lines.

Earlier studies demonstrated that MDAMB231 are genetically heterogeneous and *in vitro* selection for more aggressive populations with altered genome structure have been reported[38]. Similarly, *in vivo* growth of MDAMB231 selects for highly metastatic sublines enriched in pre-existing or newly arising genetic variants such as BRAF and KRAS[39] as well as ALPK2 and RYR1[40] that correlate with high organ specific metastatic ability. One of the key observations of this study was the increased metastatic properties of PML deficient MDAMB231 cells to various sites and a stronger preference for the development of lung metastasis. Previous studies have identified a group of genes in MDAMB231 cells expressed at higher levels in cell lines derived from lung metastases (lung metastasis signature, LMS) relative to their parental cell line[14]. The differentially expressed PML KD genes and the LMS list contains 11 common genes (Shown in Table S2). Interestingly FSCN1 and ID1 showed a change in their expression pattern resembling that of LMS. The ID gene family has important roles in development and their deregulated expression is connected to poor prognosis. Increased expression of ID1 has been associated with both primary tumor formation and lung colonization[41] presumably via mesenchymal -epithelial transition essential for the latter process[42] . The role and interaction of PML with EMT factors seems to be complex. Cytoplasmic PML promotes EMT via potentiation of TGF-b signalling[43,44]. We found here that both bHLH (TWIST) and Zn-finger (SNAIL) type EMT factors bind to and co-localize to PML IV and to a lesser extent PML I and III driven nuclear bodies. Interaction with TWIST2 requires the presence of the bHLH domain and may result in altered dimerization or DNA binding. Thus, PML may mimic the action of IDs and limit the activity of both HLH and non-HLH type EMT factors. In addition, PML KD leads to increased TWIST2 protein expression in parental tumors and the lung metastases.

Conclusions

Collectively PML impedes tumorigenicity by regulating the mesenchymal-invasive and angiogenic properties and the metastatic tropism of MDAMB231 cells. In addition PML may control the long term survival of TICs. Finally, PML loss may accelerate *in vivo* evolution of genetically heterogeneous population to acquire a more aggresive-metastatic phenotype. Mechanistically this is linked to the long term maintaining of tumor initiating cells, potentiation of their mesenchymal phenotype and a hypoxia-angiogenic switch. Hence, PML expression may serve as a valuable cancer biomarker.

Data Availability Statement

RNA-seq datasets have been deposited in SRA database under accession number PRJNA826854.

Acknowledgements

We would like to thank E.Tachmatzidi and O.Galanopoulou for helping with the *in vivo* experiments. We would also like to thank G.Vretzos and D.Tsoukatou for technical assistance, as well as the Genomic Facility of IMBB for the gene expression profiling, the Confocal Microscopy Facility and High Content Screening Facility of IMBB for imaging and data analysis respectively. We also thank M.Dimakopoulou, I.Charatsidou and C.Fountas for helping with this work.

Conflict of interest

The authors declare no conflicts of interest.

Author contributions

AV designed and performed experiments, data analysis, discussion and writing; SS, NS and TM contributed to the experimental work and discussion; ED performed immunohistochemistry in paraffin sections and histological analysis; CN performed bioinformatic analysis; AK contributed to discussion and writing; JP supervised the study and contributed to writing.

Funding

The authors of this work were funded by “DINNESMIN-MIS 5032840”, “EDBM103-MIS 5048184” and IMBB-FORTH internal funding.

Supplementary information is available at “*Supplementary Data.pdf file*”

References

1. Harbeck, N.; Penault-Llorca, F.; Cortes, J.; Gnant, M.; Houssami, N.; Poortmans, P.; Ruddy, K.; Tsang, J.; Cardoso, F. *Breast Cancer*; 2019; Vol. 5; ISBN 0123456789.
2. Lüönd, F.; Tiede, S.; Christofori, G. Breast Cancer as an Example of Tumour Heterogeneity and Tumour Cell Plasticity during Malignant Progression. *Br J Cancer* **2021**, *125*, 164–175, doi:10.1038/s41416-021-01328-7.
3. Kakizuka, A.; Miller, W.H.J.; Umesono, K.; Warrell, R.P.J.; Frankel, S.R.; Murty, V. V; Dmitrovsky, E.; Evans, R.M. Chromosomal Translocation t(15;17) in Human Acute Promyelocytic Leukemia Fuses RAR Alpha with a Novel Putative Transcription Factor, PML. *Cell* **1991**, *66*, 663–674, doi:10.1016/0092-8674(91)90112-c.
4. de Thé, H.; Lavau, C.; Marchio, A.; Chomienne, C.; Degos, L.; Dejean, A. The PML-RAR Alpha Fusion MRNA Generated by the t(15;17) Translocation in Acute Promyelocytic Leukemia Encodes a Functionally Altered RAR. *Cell* **1991**, *66*, 675–684, doi:10.1016/0092-8674(91)90113-d.
5. Hoischen, C.; Monajembashi, S.; Weisshart, K.; Hemmerich, P. Multimodal Light Microscopy Approaches to Reveal Structural and Functional Properties of Promyelocytic Leukemia Nuclear Bodies. *Front Oncol* **2018**, *8*, 125, doi:10.3389/fonc.2018.00125.
6. Hsu, K.-S.; Kao, H.-Y. PML: Regulation and Multifaceted Function beyond Tumor Suppression. *Cell Biosci* **2018**, *8*, 5, doi:10.1186/s13578-018-0204-8.
7. Li, W.; Ferguson, B.J.; Khaled, W.T.; Tevendale, M.; Stingl, J.; Poli, V.; Rich, T.; Salomoni, P.; Watson, C.J. PML Depletion Disrupts Normal Mammary Gland Development and Skews the Composition of the Mammary Luminal Cell Progenitor Pool. *Proc Natl Acad Sci U S A* **2009**, *106*, 4725–4730, doi:10.1073/pnas.0807640106.
8. Hadjimichael, C.; Chanoumidou, K.; Nikolaou, C.; Klonizakis, A.; Theodosi, G.I.; Makatounakis, T.; Papamatheakis, J.; Kretsovali, A. Promyelocytic Leukemia Protein Is an Essential Regulator of Stem Cell Pluripotency and Somatic Cell Reprogramming. *Stem Cell Reports* **2017**, *8*, 1366–1378, doi:10.1016/j.stemcr.2017.03.006.
9. Gurrieri, C.; Capodieci, P.; Bernardi, R.; Scaglioni, P.P.; Nafa, K.; Rush, L.J.; Verbel, D.A.; Cordon-Cardo, C.; Pandolfi, P.P. Loss of the Tumor Suppressor PML in Human Cancers of Multiple Histologic Origins. *J Natl Cancer Inst* **2004**, *96*, 269–279, doi:10.1093/jnci/djh043.
10. Reineke, E.L.; Kao, H.-Y. PML: An Emerging Tumor Suppressor and a Target with Therapeutic Potential. *Cancer Ther* **2009**, *7*, 219–226.
11. Sachini, N.; Arampatzi, P.; Klonizakis, A.; Nikolaou, C.; Makatounakis, T.; Lam, E.W.-F.; Kretsovali, A.; Papamatheakis, J. Promyelocytic Leukemia Protein (PML) Controls Breast Cancer Cell Proliferation by Modulating Forkhead Transcription Factors. *Mol Oncol* **2019**, *13*, 1369–1387, doi:10.1002/1878-0261.12486.
12. Ito, K.; Carracedo, A.; Weiss, D.; Arai, F.; Ala, U.; Avigan, D.E.; Schafer, Z.T.; Evans, R.M.; Suda, T.; Lee, C.H.; et al. A PML-PPAR-δ Pathway for Fatty Acid Oxidation Regulates Hematopoietic Stem Cell Maintenance. *Nat Med* **2012**, *18*, 1350–1358, doi:10.1038/nm.2882.
13. Ito, K.; Bernardi, R.; Morotti, A.; Matsuoka, S.; Saglio, G.; Ikeda, Y.; Rosenblatt, J.; Avigan, D.E.; Teruya-Feldstein, J.; Pandolfi, P.P. PML Targeting Eradicates Quiescent Leukaemia-Initiating Cells. *Nature* **2008**, *453*, 1072–1078, doi:10.1038/nature07016.

14. Minn, A.J.; Gupta, G.P.; Siegel, P.M.; Bos, P.D.; Shu, W.; Giri, D.D.; Viale, A.; Olshen, A.B.; Gerald, W.L.; Massagué, J. Genes That Mediate Breast Cancer Metastasis to Lung. *Nature* **2005**, *436*, 518–524, doi:10.1038/nature03799.

15. Gialitakis, M.; Arampatzi, P.; Makatounakis, T.; Papamatheakis, J. Gamma Interferon-Dependent Transcriptional Memory via Relocalization of a Gene Locus to PML Nuclear Bodies. *Mol Cell Biol* **2010**, *30*, 2046–2056, doi:10.1128/MCB.00906-09.

16. Zhou, B.P.; Deng, J.; Xia, W.; Xu, J.; Li, Y.M.; Gunduz, M.; Hung, M.-C. Dual Regulation of Snail by GSK-3beta-Mediated Phosphorylation in Control of Epithelial-Mesenchymal Transition. *Nat Cell Biol* **2004**, *6*, 931–940, doi:10.1038/ncb1173.

17. Arampatzi, P.; Gialitakis, M.; Makatounakis, T.; Papamatheakis, J. Gene-Specific Factors Determine Mitotic Expression and Bookmarking via Alternate Regulatory Elements. *Nucleic Acids Res* **2013**, *41*, 2202–2215, doi:10.1093/nar/gks1365.

18. Everett, R.D.; Rechter, S.; Papior, P.; Tavalai, N.; Stamminger, T.; Orr, A. PML Contributes to a Cellular Mechanism of Repression of Herpes Simplex Virus Type 1 Infection That Is Inactivated by ICP0. *J Virol* **2006**, *80*, 7995–8005, doi:10.1128/JVI.00734-06.

19. Stewart, S.A.; Dykxhoorn, D.M.; Palliser, D.; Mizuno, H.; Yu, E.Y.; An, D.S.; Sabatini, D.M.; Chen, I.S.Y.; Hahn, W.C.; Sharp, P.A.; et al. Lentivirus-Delivered Stable Gene Silencing by RNAi in Primary Cells. *RNA* **2003**, *9*, 493–501, doi:10.1261/rna.2192803.

20. Reimand, J.; Arak, T.; Adler, P.; Kolberg, L.; Reisberg, S.; Peterson, H.; Vilo, J. G:Profiler-a Web Server for Functional Interpretation of Gene Lists (2016 Update). *Nucleic Acids Res* **2016**, *44*, W83-9, doi:10.1093/nar/gkw199.

21. Drakos, E.; Leventaki, V.; Schlette, E.J.; Jones, D.; Lin, P.; Medeiros, L.J.; Rassidakis, G.Z. C-Jun Expression and Activation Are Restricted to CD30+ Lymphoproliferative Disorders. *Am J Surg Pathol* **2007**, *31*, 447–453, doi:10.1097/01.pas.0000213412.25935.e4.

22. Tomayko, M.M.; Reynolds, C.P. Determination of Subcutaneous Tumor Size in Athymic (Nude) Mice. *Cancer Chemother Pharmacol* **1989**, *24*, 148–154, doi:10.1007/BF00300234.

23. Borgna, S.; Armellin, M.; di Gennaro, A.; Maestro, R.; Santarosa, M. Mesenchymal Traits Are Selected along with Stem Features in Breast Cancer Cells Grown as Mammospheres. *Cell Cycle* **2012**, *11*, 4242–4251, doi:10.4161/cc.22543.

24. Al-Hajj, M.; Wicha, M.S.; Benito-Hernandez, A.; Morrison, S.J.; Clarke, M.F. Prospective Identification of Tumorigenic Breast Cancer Cells. *Proc Natl Acad Sci U S A* **2003**, *100*, 3983–3988, doi:10.1073/pnas.0530291100.

25. Thakur, R.; Trivedi, R.; Rastogi, N.; Singh, M.; Mishra, D.P. Inhibition of STAT3, FAK and Src Mediated Signaling Reduces Cancer Stem Cell Load, Tumorigenic Potential and Metastasis in Breast Cancer. *Sci Rep* **2015**, *5*, 10194, doi:10.1038/srep10194.

26. Qin, J.-J.; Yan, L.; Zhang, J.; Zhang, W.-D. STAT3 as a Potential Therapeutic Target in Triple Negative Breast Cancer: A Systematic Review. *J Exp Clin Cancer Res* **2019**, *38*, 195, doi:10.1186/s13046-019-1206-z.

27. Cimino, A.; Halushka, M.; Illei, P.; Wu, X.; Sukumar, S.; Argani, P. Epithelial Cell Adhesion Molecule (EpCAM) Is Overexpressed in Breast Cancer Metastases. *Breast Cancer Res Treat* **2010**, *123*, 701–708, doi:10.1007/s10549-009-0671-z.

28. Ye, F.; Zhong, X.; Qiu, Y.; Yang, L.; Wei, B.; Zhang, Z.; Bu, H. CD49f Can Act as a Biomarker for Local or Distant Recurrence in Breast Cancer. *J Breast Cancer* **2017**, *20*, 142–149,

doi:10.4048/jbc.2017.20.2.142.

29. Sheridan, C.; Kishimoto, H.; Fuchs, R.K.; Mehrotra, S.; Bhat-Nakshatri, P.; Turner, C.H.; Goulet, R.J.; Badve, S.; Nakshatri, H. CD44+/CD24- Breast Cancer Cells Exhibit Enhanced Invasive Properties: An Early Step Necessary for Metastasis. *Breast Cancer Res* **2006**, *8*, R59, doi:10.1186/bcr1610.

30. Meyer, M.J.; Fleming, J.M.; Ali, M.A.; Pesesky, M.W.; Ginsburg, E.; Vonderhaar, B.K. Dynamic Regulation of CD24 and the Invasive, CD44posCD24neg Phenotype in Breast Cancer Cell Lines. *Breast Cancer Res* **2009**, *11*, R82, doi:10.1186/bcr2449.

31. Idowu, M.O.; Kmieciak, M.; Dumur, C.; Burton, R.S.; Grimes, M.M.; Powers, C.N.; Manjili, M.H. CD44(+)/CD24(-/Low) Cancer Stem/Progenitor Cells Are More Abundant in Triple-Negative Invasive Breast Carcinoma Phenotype and Are Associated with Poor Outcome. *Hum Pathol* **2012**, *43*, 364–373, doi:10.1016/j.humpath.2011.05.005.

32. Fillmore, C.M.; Kuperwasser, C. Human Breast Cancer Cell Lines Contain Stem-like Cells That Self-Renew, Give Rise to Phenotypically Diverse Progeny and Survive Chemotherapy. *Breast Cancer Res* **2008**, *10*, R25, doi:10.1186/bcr1982.

33. Xie, Y.; Li, J.; Zhang, C. STAT3 Promotes the Proliferation and Migration of Hepatocellular Carcinoma Cells by Regulating AKT2. *Oncol Lett* **2018**, *15*, 3333–3338, doi:10.3892/ol.2017.7681.

34. Bernardi, R.; Guernah, I.; Jin, D.; Grisendi, S.; Alimonti, A.; Teruya-Feldstein, J.; Cordon-Cardo, C.; Simon, M.C.; Rafii, S.; Pandolfi, P.P. PML Inhibits HIF-1alpha Translation and Neoangiogenesis through Repression of MTOR. *Nature* **2006**, *442*, 779–785, doi:10.1038/nature05029.

35. Ponente, M.; Campanini, L.; Cuttano, R.; Piunti, A.; Delledonne, G.A.; Coltella, N.; Valsecchi, R.; Villa, A.; Cavallaro, U.; Pattini, L.; et al. PML Promotes Metastasis of Triple-Negative Breast Cancer through Transcriptional Regulation of HIF1A Target Genes. *JCI insight* **2017**, *2*, e87380, doi:10.1172/jci.insight.87380.

36. Martín-Martín, N.; Piva, M.; Urosevic, J.; Aldaz, P.; Sutherland, J.D.; Fernández-Ruiz, S.; Arreal, L.; Torrano, V.; Cortazar, A.R.; Planet, E.; et al. Stratification and Therapeutic Potential of PML in Metastatic Breast Cancer. *Nat Commun* **2016**, *7*, 12595, doi:10.1038/ncomms12595.

37. Arreal, L.; Piva, M.; Fernández, S.; Revandkar, A.; Schaub-Clerigué, A.; Villanueva, J.; Zabala-Letona, A.; Pujana, M.; Astobiza, I.; Cortazar, A.R.; et al. Targeting PML in Triple Negative Breast Cancer Elicits Growth Suppression and Senescence. *Cell Death Differ* **2020**, *27*, 1186–1199, doi:10.1038/s41418-019-0407-5.

38. Amaro, A.; Angelini, G.; Mirisola, V.; Esposito, A.I.; Reverberi, D.; Matis, S.; Maffei, M.; Giaretti, W.; Viale, M.; Gangemi, R.; et al. A Highly Invasive Subpopulation of MDA-MB-231 Breast Cancer Cells Shows Accelerated Growth, Differential Chemoresistance, Features of Apocrine Tumors and Reduced Tumorigenicity in Vivo. *Oncotarget* **2016**, *7*, 68803–68820, doi:10.18632/oncotarget.11931.

39. Jacob, L.S.; Vanharanta, S.; Obenauf, A.C.; Pirun, M.; Viale, A.; Socci, N.D.; Massagué, J. Metastatic Competence Can Emerge with Selection of Preexisting Oncogenic Alleles without a Need of New Mutations. *Cancer Res* **2015**, *75*, 3713–3719, doi:10.1158/0008-5472.CAN-15-0562.

40. Jiang, Y.; Qiu, Y.; Minn, A.J.; Zhang, N.R. Assessing Intratumor Heterogeneity and Tracking Longitudinal and Spatial Clonal Evolutionary History by Next-Generation Sequencing. *Proc Natl*

Acad Sci **2016**, *113*, E5528 LP-E5537, doi:10.1073/pnas.1522203113.

41. Gupta, G.P.; Perk, J.; Acharyya, S.; de Candia, P.; Mittal, V.; Todorova-Manova, K.; Gerald, W.L.; Brogi, E.; Benezra, R.; Massagué, J. ID Genes Mediate Tumor Reinitiation during Breast Cancer Lung Metastasis. *Proc Natl Acad Sci U S A* **2007**, *104*, 19506–19511, doi:10.1073/pnas.0709185104.

42. Stankic, M.; Pavlovic, S.; Chin, Y.; Brogi, E.; Padua, D.; Norton, L.; Massagué, J.; Benezra, R. TGF-β-Id1 Signaling Opposes Twist1 and Promotes Metastatic Colonization via a Mesenchymal-to-Epithelial Transition. *Cell Rep* **2013**, *5*, 1228–1242, doi:10.1016/j.celrep.2013.11.014.

43. Buczek, M.E.; Miles, A.K.; Green, W.; Johnson, C.; Boocock, D.J.; Pockley, A.G.; Rees, R.C.; Hulman, G.; van Schalkwyk, G.; Parkinson, R.; et al. Cytoplasmic PML Promotes TGF-β-Associated Epithelial–Mesenchymal Transition and Invasion in Prostate Cancer. *Oncogene* **2016**, *35*, 3465–3475, doi:10.1038/onc.2015.409.

44. Lin, H.; Bergmann, S.; Pandolfi, P.P. Cytoplasmic PML Function in TGF- b Signalling. **2004**, *431*, 205–211, doi:10.1038/nature02866.Published.